CONF-970572--1 SAN097-0243C
SAND--97-0243C
to be submitted to: InP and Related Materials Conf. May 11-15, 1997 Hyannis, MA (Invited)

InAlGaP Vertical Cavity Surface Emitting Lasers (VCSELs): Processing and Performance

M. Hagerott Crawford*, K. D. Choquette, R. J. Hickman, and K. M. Geib
Sandia National Laboratories, Albuquerque, NM, 87185-0601
* e-mail: mhcrawf@sandia.gov

Introduction

$(Al_yGa_{1-y})_{1-x}In_xP$ semiconductor alloys lattice-matched to GaAs are widely used in visible optoelectronic devices. One of the most recent developments in this area is the AlGaInP-based red vertical cavity surface emitting laser (VCSEL) [1,2]. These lasers, which employ AlGaInP active regions and AlGaAs distributed Bragg reflectors (DBRs), have demonstrated continuous-wave (CW) lasing over the 630-690 nm region of the spectrum [2,3]. Applications for these lasers include plastic fiber data communications, laser printing and bar code scanning. In this paper, we present an overview of recent developments in the processing and performance of AlGaInP based VCSELs. This overview will include a review of the general heterostructure designs that have been employed, as well as the performance of lasers fabricated by both ion implantation and selective oxidation.

I. General Heterostructure design of AlGaInP VCSELs

The general design for the visible VCSEL active region is similar to that which has been employed in AlGaInP edge emitting lasers. It includes compressively strained $In_{0.56}Ga_{0.44}P$ quantum wells with $(Al_yGa_{1-y})_{0.5}In_{0.5}P$ barriers and cladding layers. The quantum well thickness is typically 70 Å with 65 Å barriers. The one wave thick cavity is approximately 2000 Å for the 670 nm region. A schematic of the active region is shown in Figure 1.

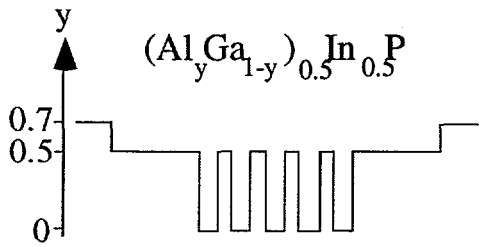

Figure 1: Heterostructure design for AlGaInP based visible VCSEL active region

The DBRs for the visible VCSELs are $Al_xGa_{1-x}As$ alloys and typically x=0.5 alloys have been used for the high index layer and x=0.92-1 alloys have been used for the low index layers . Bi-parabolic grading of the alloy composition is employed between the layers to reduce the resistance of the mirrors. For these top emitting devices, up to 36 high and low index layer pairs are used in the top DBR and 55.5 pairs are used in the bottom DBR [1, 2, 8].

II. Processing of Visible VCSELs

The most conventional VCSEL structure is a planar design utilizing ion implantation to define the current aperture of the lasers and to provide isolation from neighboring devices. Significant advances in the performance of both near-IR and visible VCSELs have been realized by employing an alternate fabrication technique, namely selective oxidation, in the processing of the VCSEL [3-8]. This technique involves the preferential oxidation of one or more relatively high aluminum containing AlGaAs layers in the DBRs near the active region of the device. In the visible VCSEL design, the low index layer of the top DBR pair closest to the cavity is typically $Al_xGa_{1-x}As$ with x=0.98 and x=0.95 is typically used for the remaining low index layers. One to five x=0.98 layers have been employed in a given design.

In the selective oxidation process, mesas are fabricated by dry etching down to the AlGaInP layers. The devices are oxidized in a wet steam furnace at 440 °C with an oxidation rate of approximately 0.8 μm/min.

DISCLAIMER

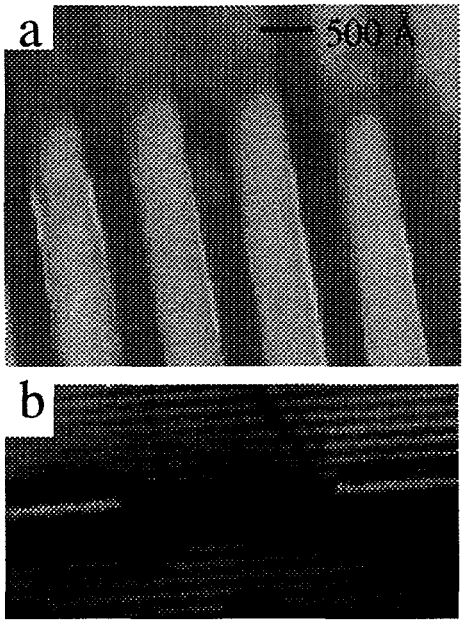

Figure :2 TEM images of a) edges of four oxide layers and b) oxide defined aperture in near-cavity region of a selectively oxidized VCSEL. The oxide aperture in (b) is approximately 3 μm.

TEM images of oxidized visible VCSELs are shown in Figure 2. In Figure 2a, we show the edges of four neighboring oxidized layers, demonstrating the sharp definition of the oxide layers. Figure 2b shows a single oxidized layer above the AlGaInP cavity, where the aperture created by the oxide layer is approximately 3 μm. Nearby regions of the top and bottom DBR are also seen in the image. The thin (500 Å) and low index (n = 1.55) aluminum-oxide layer serves to provide both electrical and optical confinement and can enable well defined device diameters as small as 1 μm.

III. Performance of Visible VCSELs

The performance of visible VCSELs has advanced markedly over the past several years. State of the art performance includes the demonstration of 2 mW single mode power at 690 nm, > 8 mW multimode at 690 nm and up to 11 % wallplug efficiency from ion implanted devices [2]. Selectively oxidized devices have been demonstrated with reduced threshold conditions (Ith < 1 mA) [8] as compared to ion implanted structures and with CW lasing down to 630 nm [3]. In this section, we review further advances that have been made with improvements in heterostructure design and selective oxidation.

A. High Temperature Performance of Ion Implanted and Selectively Oxidized VCSELs

One of the areas in which visible VCSEL performance has lagged behind that of near-IR VCSELs is in high temperature performance. Achieving CW lasing from visible VCSELs at elevated temperatures is challenging due to enhanced carrier leakage in the AlGaInP-based active region [9] as compared to the GaAs and InGaAs quantum well active regions of 850 nm and 980 nm VCSELs, respectively .

While previously reported visible VCSEL designs incorporated $(Al_{0.5}Ga_{0.5})_{0.5}In_{0.5}P$ barrier layers with no cladding layers [2], recent designs have included higher bandgap $(Al_{0.7}Ga_{0.3})_{0.5}In_{0.5}P$ cladding layers, as shown schematically in Figure 1. The temperature dependent performance of both implanted and selectively oxidized structures incorporating this design have been evaluated.

In Figure 3, we show temperature dependent light output power-current-voltage (L-I-V) data for a 10 μm diameter ion implanted VCSEL employing the higher bandgap $(Al_{0.7}Ga_{0.3})_{0.5}In_{0.5}P$ cladding layers. The lasing wavelength is 677 nm at 25°C. The VCSEL structure has a cavity mode/ gain peak offset of approximately 7 nm to improve performance above room temperature, although the design was not specifically optimized for high temperature performance. CW lasing up to 75 °C has been achieved with a change in peak power with temperature of -0.029 mW/°C. Exact comparison with previously reported data on devices which do not employ the $(Al_{0.7}Ga_{0.3})_{0.5}In_{0.5}P$ cladding layers is difficult due to the fact that the optimized devices were 15 μm in diameter with emission at 690 nm. However, best performance previously achieved in these structures demonstrated a -0.075 mW/°C peak power change with temperature and CW lasing up to 60 °C [2].

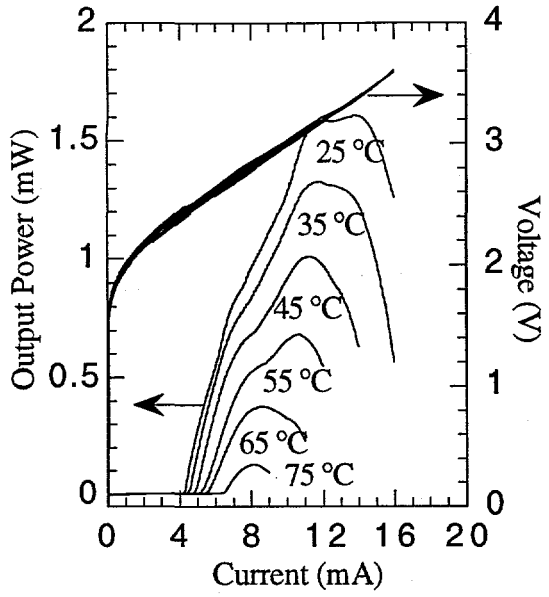

Figure 3: Temperature dependent L-I-V data for an ion implanted VCSEL with $(Al_{0.7}Ga_{0.3})_{0.5}In_{0.5}P$ cladding layers.

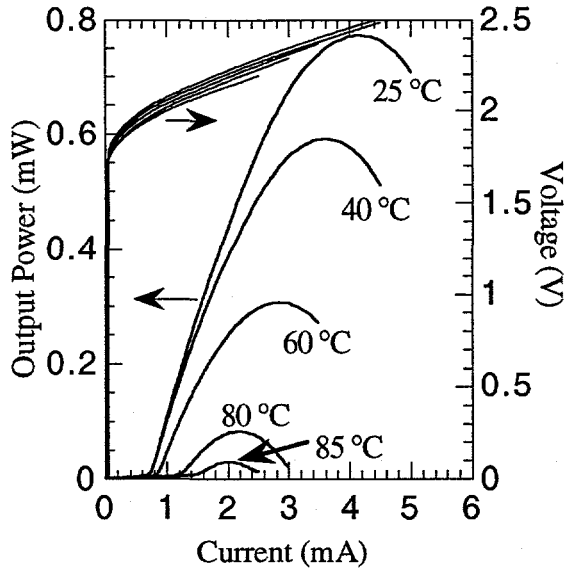

Figure 4: Temperature dependent L-I-V data for a selectively oxidized VCSEL with $(Al_{0.7}Ga_{0.3})_{0.5}In_{0.5}P$ cladding layers.

Selectively oxidized visible VCSELs have the potential to achieve CW lasing at even higher temperatures, due to their high efficiency and low input power requirements. As an example, in Figure 4, we show the performance of a 3 μm x 3 μm selectively oxidized VCSEL with a similar active region as the ion implanted device represented in Figure 3. The lasing wavelength is 683 nm at 25 °C. Although the maximum output power of the device is less, CW lasing up to 85 °C is achieved and low threshold voltages of 2.0 V over the 25-80 °C temperature range are seen. The drop in peak power with temperature is slightly less than for the ion implanted structure, namely -0.0125 mW/°C.

B. Low Threshold Performance of Selectively Oxidized VCSELs

The small volumes and enhanced electrical and optical confinement provided by selective oxidation has resulted in improved threshold performance and wallplug efficiencies for both visible [8] and IR VCSELs [10-12]. Recent work on red VCSELs has included design changes to improve these properties. As previously mentioned, applying $(Al_{0.7}Ga_{0.3})_{0.5}In_{0.5}P$ cladding layers was performed to reduce carrier leakage. Another area of device design that was explored was the number of oxide layers above the active region. Previous designs employed 5 oxide layers [8], while fewer pairs are expected to improve performance due to reduced scattering loss.

In Figure 5, we present L-I-V data of a design employing 2 oxide layers above the AlGaInP cavity. A low threshold voltage of 1.980 V (only 135 meV above the photon energy) has been achieved. This device also demonstrates a relatively low threshold current of 0.6 mA and a peak wallplug efficiency of 12.2%, the highest value reported for visible VCSELs.

We have also explored the performance of selectively oxidized VCSELs with varying top mirror reflectivity. The devices previously mentioned have employed 34 top mirror pairs, which results in a top mirror reflectivity of approximately 0.9981. CW lasing has been achieved with structures employing 28-36 mirror pairs, with an effective range of reflectivity of 0.9948-0.9986. In Figure 6, we show L-I-V data from a 2 μm x 3 μm selectively oxidized VCSEL with 36 top mirror pairs. The device demonstrates a low threshold current of 0.38 mA and a threshold voltage of 2.10 volts.

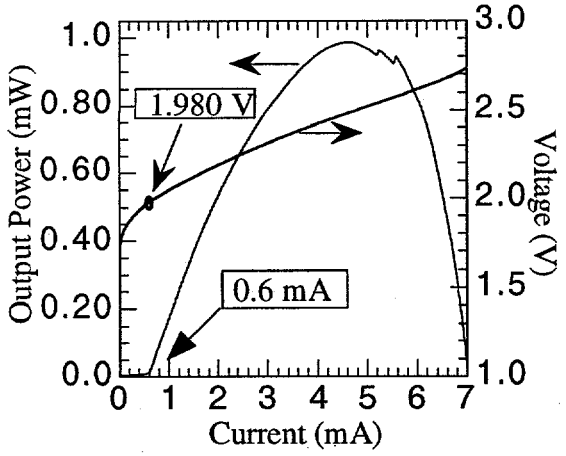

Figure 5: L-I-V data for a 3 μm x 3 μm selectively oxidized visible VCSEL with 34 top DBR pairs and emission at 672 nm.

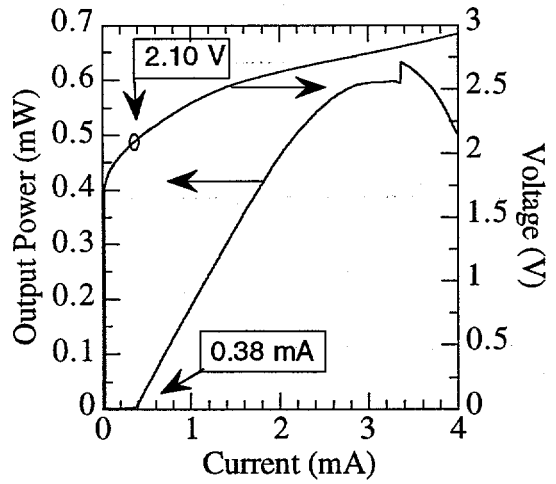

Figure 6: L-I-V data for a 2 μm x 3 μm selectively oxidized VCSEL with 36 top mirror pairs. Emission is at 673 nm.

IV. Conclusions

The performance of AlGaInP based visible VCSELs has been advanced with the application of new heterostructure designs and the technique of selective oxidation. Improved performance at elevated temperatures as well as high wallplug efficiency, low threshold devices have been demonstrated for devices operating in the 670-680 nm region. Challenges still remain in demonstrating high performance devices with emission wavelengths shorter than 650 nm.

Acknowledgments

The authors gratefully acknowledge Dave Mathes and Robert Hull from the University of Virginia for providing TEM images of selectively oxidized VCSELs. Technical discussions with Kevin Lear and Hong Hou of Sandia National Labs and Richard Schneider of Hewlett Packard Labs are also acknowledged. This work has been supported by the United States Department of Energy under Contract DE-AC04-94AL85000. Sandia is a multiprogram laboratory operated by Sandia Corporation, a Lockheed Martin Company, for the United States Department of Energy.

References

[1] R. P. Schneider, Jr., K. D. Choquette, J. A. Lott, K. L. Lear, J. J. Figiel and K. J. Malloy, *IEEE Photon. Tech. Lett.*, vol. 6, pp. 313-316, 1994.

[2] M. H. Crawford, R. P. Schneider, Jr., K. D. Choquette and K. L. Lear, *IEEE Photon. Technol. Lett.*, vol. 7, pp. 724-726, 1995.

[3] J. A. Lott, L. V. Buydens, K. J. Malloy, K. Kobayashi and S. Ishikawa, Inst. Phys. Conf. Ser.. vol. 145, pp. 973-976, 1996.

[4] D. L. Huffaker, D. G. Deppe and K. Kumar, , *Appl. Phys. Lett.*, vol. 65, pp. 97-99, 1994.

[5] K. D. Choquette, R. P. Schneider, Jr., K. L. Lear and K. M. Geib, *Electron. Lett.*, vol. 30, pp. 2043-2044, 1994.

[6] Y. Hayashi, T. Mukaihara, N. Hatori, N. Ohnoki, A. Matsutani, F. Koyama and K. Iga, *Electron. Lett.*, vol. 31, pp. 560-562, 1995.

[7] G. M. Yang, M. H. MacDougal and P. D. Dapkus, *Electron. Lett.*, vol. 31, pp. 886-888, 1995.

[8] K. D. Choquette, R. P. Schneider, M. H. Crawford, K. M. Geib and J. J. Figiel, *Electron. Lett.*, vol. 31, pp. 1145-1146, 1995.

[9] D. P. Bour, D. W. Treat, R. L. Thornton, R. S. Geels, and D. F. Welch, *IEEE J. Quantum Electron., vol. 29*, pp. 1337-1342, 1993.

[10] K. L. Lear, K. D. Choquette, R. P. Schneider, Jr., S. P. Kilcoyne and K. M. Geib, *Electron. Lett.*, vol. 31, pp. 208-209, 1995.

[11] B. Weigl, M. Grabherr, G. Reiner and K. J. Ebeling, *Electron. Lett.*, vol. 32, pp. 557-558, 1996.

[12] B. Weigl, G. Reiner, M. Grabherr, K. J. Ebeling, *Electron. Lett.*, vol. 32, pp1784-1786, 1996.